

See discussions, stats, and author profiles for this publication at: <https://www.researchgate.net/publication/312558387>

A simply designed and universal sliding mode observer for the SOC estimation of Lithium-ion batteries

Article in IET Power Electronics · January 2017

DOI: 10.1049/iet-pel.2016.0095

CITATIONS
34

READS
8,822

4 authors, including:



Jiuchun Jiang
Beijing Jiaotong University
228 PUBLICATIONS 9,206 CITATIONS

[SEE PROFILE](#)



Haijun Ruan
Imperial College London
46 PUBLICATIONS 1,327 CITATIONS

[SEE PROFILE](#)



Caiping Zhang
Beijing Jiaotong University
125 PUBLICATIONS 4,855 CITATIONS

[SEE PROFILE](#)

Simply designed and universal sliding mode observer for the SOC estimation of lithium-ion batteries

Qiaoyan Chen^{1,2} , Jiuchun Jiang^{1,2}, Haijun Ruan^{1,2}, Caiping Zhang^{1,2}

¹National Active Distribution Network Technology Research Center (NANTEC), School of Electrical Engineering, Beijing Jiaotong University, No. 3 Shang Yuan Cun, Haidian District, 100044 Beijing, People's Republic of China

²Collaborative Innovation Center of Electric Vehicles in Beijing, No. 3 Shang Yuan Cun, Haidian District, 100044 Beijing, People's Republic of China

 E-mail: tianjincqy@163.com

Abstract: A new sliding mode observer to estimate the state of charge (SOC) of lithium-ion batteries is presented. The proposed observer has been developed from a previous observer. The observer is applicable to the common battery circuit models and the design of the algorithm is simple. The observer can also be used for state estimations of both time-varying and time-invariant systems. The robustness of the observer is proved by Lyapunov stability theory. In this study, two typical circuit models are used as examples to design the observer and this study shows that the design of the observer is simple and the observer exhibits good performance. The observer is used to estimate the battery SOC under two conditions. The estimation results show that the observer is robust and the adaptive method can improve the estimation accuracy.

1 Introduction

Lithium-ion batteries, as energy storage tools, are widely applied for its high-energy density, high-power density and long life. Battery management system can fully play the battery performance as well as lengthen its lifetime and the state of charge (SOC) estimation is the basis of battery management.

The working process of the battery is a complicated physical and chemical reaction process, which results in the strong non-linear and uncertainty features of the battery, so the SOC estimation is difficult. The current integration is a simple SOC estimation method, but the estimation error will be accumulated as time goes on, and this method also needs the initial SOC [1, 2]; the Kalman filter is based on the accurate battery model, but it is difficult to get the noise covariance of the model [3–6]; the open-circuit voltage (OCV) method needs the battery to be static for a period of time after being used, which is unsuitable for the real-time SOC estimation [7]; the neural network involves lots of training with a large amount of data, and the accuracy of the SOC estimation is related to the samples and training methodology [8–11]; the electrochemical impedance spectroscopy needs external excitation source which can send out multi-frequency excitation signal [12]; the H_∞ observer is robust to the battery state-space equations, but the observer design and calculation is complex [13]; the approximate least squares [14] and the method of analysis and calculation after current interruption [15] require many fitting curves, and thus the two methods are limited by the fitting conditions. Besides, the calculations of the two methods are complicated.

Siding mode observer is a non-linear observer and it is robust in SOC estimation. In addition, the observer can estimate SOC in real-time, so it has attracted more and more attention [16–24].

There are two forms of battery state equations: the matrix form and the equations form. Accordingly, there are two main design forms of the sliding mode observer for SOC estimation. (i) If the battery state equation is in the form of matrix, the observer is designed in the matrix form, but this design method needs to solve matrix equations which will make the design complicated [16–19]. (ii) If the battery state equation is in the form of equations, based on each state equation of the equations, one observer for the state component is designed. This method requires designing multiple observers of the state components for the whole observer of the

state vector, so this method will be much complicated especially too many dimensions of the equations [20–24].

The design of the existing sliding mode observers used in SOC estimation is complex, leading to its inconvenience to practical application. This paper introduces a new observer as an extension of the existing observer for the SOC estimation. It does not need to solve matrix equations or design multiple observers for all state components, so it is simple in design. In addition, the observer can be applied to the common circuit models in this paper, and it exhibits good generality. Its robustness is proved by Lyapunov's stability theory. From the proof process, it can be seen that the observer is robust to both time-varying system and time-invariant system, so it also can be used for SOC estimation of changing parameters models.

Two common battery circuit models were chosen to establish state-space equations, and the sliding mode observer was designed based on the state-space equations. Through the design, it can be seen that the new observer has the advantages of simple design and good generality.

A lithium-ion battery with 25 Ah nominal capacity was chosen as the experimental subject, and was operated under the simulation Los Angeles 92 (LA92) condition. Since the battery model parameters are changing in the test, a time-varying parameter dynamic model was set up. On the basis of the time-varying parameter model and the time-invariant parameter model, the observer was designed. Using the observer for the SOC estimation under the simulation LA92 condition, the estimation results show that the new observer has good robustness, and the adaptive observer improves the accuracy of the SOC estimation.

2 Battery modelling

In the battery model, the SOC and the OCV are two important physical quantities, and there exists a functional relationship between the two physical quantities.

2.1 OCV and SOC

The battery SOC describes the battery remaining capacity, and it is defined as the ratio of battery remaining capacity to the maximum available capacity [13]. According to the definition, SOC can be expressed as

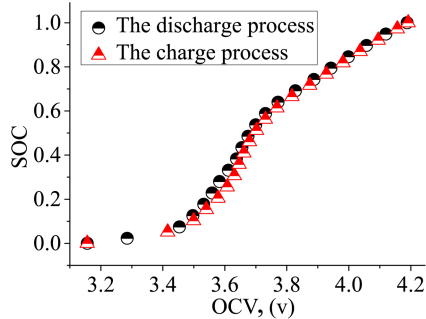


Fig. 1 Function of SOC versus OCV

$$SOC = \frac{Q_{re}}{Q_n} = SOC_0 + \frac{\int_{t_0}^t \eta i_t dt}{Q_n} \quad (1)$$

where Q_{re} is the remaining capacity, Q_n is the maximum available capacity, which can be obtained through measurement, SOC_0 is the initial SOC, η is the coulomb efficiency and i_t is the instantaneous input current, which is positive for charge current and negative for discharge current [13].

The OCV is a natural characteristic of the battery and related to the battery internal materials, and it is different during the discharge process and the charge process. The OCV data were obtained through measuring and it is shown in Fig. 1.

2.2 Battery circuit models

The common circuit models of the battery in this paper can be classified into the following two categories and the two typical models are shown in Fig. 2.

2.2.1 OCV without parallel branch: These common models include the Randle model and the Partnership for a New Generation of Vehicles (PNGV) model. Taking the former as an example, battery state-space equations are established. Fig. 2a shows the n th-order Randle circuit model [25], where V_{OC} is the OCV, R_i is the ohmic resistance, C_1, C_2, \dots, C_n and R_1, R_2, \dots, R_n reflect the charge transfer and diffusion of the battery, i_t is the input current and V_t is the terminal voltage.

According to Fig. 2a, the input current i_t can be expressed as

$$i_t = \dot{V}_k C_k + \frac{V_k}{R_k} \quad (k = 1, 2, \dots, n) \quad (2)$$

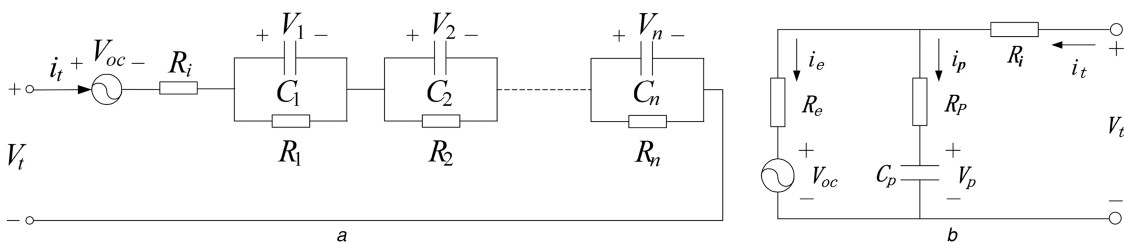


Fig. 2 Two common battery circuit models

(a) Battery n th-order Randle circuit model, (b) Battery RC circuit model

Considering the modelling error and the internal/external disturbance errors, the state equation of the k th Resistance-Capacitance (RC) parallel branch is as follows:

$$\dot{V}_k = -\frac{1}{R_k C_k} V_k + \frac{1}{C_k} i_t + f_k \quad (k = 1, 2, \dots, n) \quad (3)$$

where f_k is the abbreviation of the function $f_k(x, u, t)$ ($k = 1, 2, \dots, n$), and it is the sum of all the errors of the k th state equation, so it is a non-linear uncertain function. In mathematical expression, the error functions are always substituted with the abbreviation. Assuming the function of OCV versus SOC is $V_{OC} = L(SOC)$, where SOC is the SOC, and V_{OC} is the OCV. The state equation of the OCV can be expressed as

$$\dot{V}_{OC} = \frac{dL(SOC)}{d(SOC)} \dot{S}_{OC} = L \dot{S}_{OC} = L \frac{\eta i_t}{Q_n} \quad (4)$$

where the coefficient $L = dL(SOC)/d(SOC)$ and it varies with the SOC. For convenience, let the coefficients L and η are 1, which causes the linearisation error, and (4) results in

$$\dot{V}_{OC} = \frac{i_t}{Q_n} + f_{n+1} \quad (5)$$

where f_{n+1} is the sum of the linearisation error, modelling error and the disturbance errors.

According to (3) and (5), the battery state equation of the n th-order Randle circuit model can be expressed as (see (6)) The observation equation is as follows:

$$V_t = [1, 1, \dots, 1][V_1, V_2, \dots, V_n, V_{OC}]^T + R_i i_t \quad (7)$$

where $x = [V_1, V_2, \dots, V_n, V_{OC}]^T$ is the state vector and $f = [f_1, f_2, \dots, f_n, f_{n+1}]^T$ is the error vector. Similarly, f is the abbreviation of $f(x, u, t)$. The coefficient matrixes of the equations are

$$\begin{aligned} A &= \text{diag}\left(-\frac{1}{R_1 C_1}, -\frac{1}{R_2 C_2}, \dots, -\frac{1}{R_n C_n}, 0\right), \\ B &= \left[\frac{1}{C_1}, \frac{1}{C_2}, \dots, \frac{1}{C_n}, \frac{1}{Q_n}\right]^T, \\ C &= [1, 1, \dots, 1] \quad \text{and} \quad D = R_i. \end{aligned}$$

Equations (6) and (7) are state-space equations of the n th-order Randle circuit model. If the dimension of the circuit model is 1, the

$$\begin{bmatrix} \dot{V}_1 \\ \dot{V}_2 \\ \vdots \\ \dot{V}_n \\ \dot{V}_{OC} \end{bmatrix} = \text{diag}\left(-\frac{1}{R_1 C_1}, -\frac{1}{R_2 C_2}, \dots, -\frac{1}{R_n C_n}, 0\right) \begin{bmatrix} V_1 \\ V_2 \\ \vdots \\ V_n \\ V_{OC} \end{bmatrix} + \begin{bmatrix} 1/C_1 \\ 1/C_2 \\ \vdots \\ 1/C_n \\ 1/Q_n \end{bmatrix} i_t + \begin{bmatrix} f_1 \\ f_1 \\ \vdots \\ f_n \\ f_{n+1} \end{bmatrix} \quad (6)$$

circuit model is the Thevenin circuit model, and if the dimension is 2, it is the second-order circuit model.

2.2.2 OCV with parallel branch: These common models include the RC circuit model and the General Nonlinear Model (GNL) model, whose coefficient matrix A is not diagonal matrix. The RC circuit model is shown in Fig. 2b [30], where V_{OC} is the OCV, R_e is the propagation resistor, C_p and R_p are the polarisation capacitance and diffused resistor, V_p is the polarised voltage, R_i is the ohmic resistance, i_t is the input current and V_t is the battery terminal voltage. The state equation of RC circuit model can be expressed as [26]

$$\begin{bmatrix} \dot{V}_p \\ \dot{V}_{oc} \end{bmatrix} = \begin{bmatrix} -\frac{1}{C_p(R_e + R_p)} & \frac{1}{C_p(R_e + R_p)} \\ \frac{1}{Q_n(R_e + R_p)} & -\frac{1}{Q_n(R_e + R_p)} \end{bmatrix} \begin{bmatrix} V_p \\ V_{oc} \end{bmatrix} + \begin{bmatrix} \frac{R_e}{C_p(R_e + R_p)} \\ \frac{R_p}{Q_n(R_e + R_p)} \end{bmatrix} i_t + \begin{bmatrix} f_1 \\ f_2 \end{bmatrix} \quad (8)$$

The observation equation is [26]

$$V_t = \begin{bmatrix} R_e & R_p \\ R_e + R_p & R_e + R_p \end{bmatrix} \begin{bmatrix} V_p \\ V_{oc} \end{bmatrix} + \begin{bmatrix} R_i + \frac{R_e R_p}{R_e + R_p} \\ i_t \end{bmatrix} + \begin{bmatrix} f_1 \\ f_2 \end{bmatrix} \quad (9)$$

where $\mathbf{x} = [V_p \ V_{oc}]^T$ is the state vector, $y = V_t$ is the observation and f_1 and f_2 are the sum of the modelling errors, the linearisation errors and the errors caused by internal/external disturbance of the battery, and they are non-linear uncertain functions. Equations (8) and (9) are battery state-space equations. The coefficient matrixes of the equations are

$$\begin{aligned} \mathbf{A} &= \begin{bmatrix} -\frac{1}{C_p(R_e + R_p)} & \frac{1}{C_p(R_e + R_p)} \\ \frac{1}{Q_n(R_e + R_p)} & -\frac{1}{Q_n(R_e + R_p)} \end{bmatrix}, \quad \mathbf{B} = \begin{bmatrix} \frac{R_e}{C_p(R_e + R_p)} \\ \frac{R_p}{Q_n(R_e + R_p)} \end{bmatrix}, \\ \mathbf{C} &= \begin{bmatrix} R_e & R_p \\ R_e + R_p & R_e + R_p \end{bmatrix}, \quad \mathbf{D} = \begin{bmatrix} R_i + \frac{R_e R_p}{R_e + R_p} \\ i_t \end{bmatrix} \end{aligned}$$

3 Design of the new sliding mode observer

3.1 New sliding mode observer

If the non-linear uncertain system is as follows:

$$\dot{\mathbf{x}}(t) = \mathbf{A}\mathbf{x}(t) + \mathbf{B}\mathbf{u}(t) + \mathbf{f}(\mathbf{x}, \mathbf{u}, t) \quad (10)$$

$$\mathbf{y}(t) = \mathbf{C}\mathbf{x}(t) + \mathbf{D}\mathbf{u}(t) \quad (11)$$

where $\mathbf{A} \in R^{n \times n}$, $\mathbf{B} \in R^{n \times m}$, $\mathbf{C} \in R^{l \times n}$, $\mathbf{D} \in R^{l \times m}$, \mathbf{B} and \mathbf{C} are full rank, (\mathbf{A}, \mathbf{C}) is observable, $\mathbf{u}(t) \in R^m$ is the control variable, and $\mathbf{f} = [f_1, f_2, \dots, f_n]^T \in R^n$ is the bounded, non-linear and uncertain function vector. On the basis of the (10) and (11), the observer is designed as [27, 28]

$$\dot{\hat{\mathbf{x}}}(t) = \mathbf{A}\hat{\mathbf{x}}(t) + \mathbf{B}\mathbf{u}(t) - \mathbf{G}(\hat{\mathbf{y}}(t) - \mathbf{y}(t)) + \mathbf{B}\mathbf{v} \quad (12)$$

where $\hat{\mathbf{x}}(t) \in R^n$ is the estimation vector, $\mathbf{G} \in R^{n \times l}$ is the designed matrix and $\mathbf{v}(\hat{\mathbf{x}}, t) \in R^n \times R^+ \rightarrow R^n$ is the control variable. If the estimation error is $\mathbf{e}(t) = \hat{\mathbf{x}}(t) - \mathbf{x}(t)$, the error system can be derived from (10)–(12). The error system is as follows:

$$\dot{\mathbf{e}}(t) = \mathbf{A}_0\mathbf{e}(t) - \mathbf{f}(\mathbf{x}, \mathbf{u}, t) + \mathbf{B}\mathbf{v} \quad (13)$$

where $\mathbf{A}_0 = \mathbf{A} - \mathbf{GC}$.

The sliding mode surface is designed as [27, 28]

$$\mathbf{S} = \mathbf{F}(\hat{\mathbf{y}}(t) - \mathbf{y}(t)) = \mathbf{FC}(\hat{\mathbf{x}}(t) - \mathbf{x}(t)) = \mathbf{Me} = 0 \quad (14)$$

where \mathbf{F} and \mathbf{M} are designed coefficient matrixes and $\mathbf{M} = \mathbf{FC}$. That means the surface, on which the observation error is 0, is chosen as the sliding mode surface.

The control variable of the observer is designed as

$$\mathbf{v} = \begin{cases} -\frac{(\mathbf{S}^T \mathbf{MB})^T}{\|\mathbf{S}^T \mathbf{MB}\|^2} (\nabla_1 + \nabla_2) & \|\mathbf{S}^T \mathbf{MB}\| \neq 0 \\ 0 & \|\mathbf{S}^T \mathbf{MB}\| = 0 \end{cases} \quad (15)$$

where $\nabla_1 = \rho \mathbf{S} \mathbf{MB}$, $\nabla_2 = \eta((1/2)^\beta \mathbf{S}^{2\beta})$, η and β are coefficients, $0 \leq \eta \leq 1$, $\beta \geq 0$ and ρ is the designed coefficient.

If the following assumptions are met, the observer is robust.

Assumption 1: $\lambda_{\max}(\mathbf{A}_0) \leq 0$.

Assumption 2: $\rho \mathbf{MB} \geq \mathbf{Mf}$.

3.2 Proof of the new observer robustness

If the Lyapunov function is

$$V(\mathbf{e}) = \frac{1}{2} \mathbf{e}^T \mathbf{M}^T \mathbf{Me} = \frac{1}{2} \mathbf{S}^T \mathbf{S} = \frac{1}{2} \|\mathbf{S}\|^2 \geq 0 \quad (16)$$

then

$$\begin{aligned} \dot{V}(\mathbf{e}) &= \mathbf{S}^T \dot{\mathbf{S}} = \mathbf{e}^T \mathbf{M}^T \mathbf{Me} = \mathbf{e}^T \mathbf{M}^T \mathbf{M}(\mathbf{A}_0 \mathbf{e} - \mathbf{f} + \mathbf{Bv}) \\ \dot{V}(\mathbf{e}) &= \mathbf{e}^T \mathbf{M}^T \mathbf{M} \mathbf{A}_0 \mathbf{e} - \mathbf{S}^T \mathbf{Mf} + \mathbf{S}^T \mathbf{MBv} \\ &\leq \lambda_{\max}(\mathbf{M}^T \mathbf{M} \mathbf{A}_0) \|\mathbf{e}\|^2 - \mathbf{S}^T \mathbf{Mf} + \mathbf{S}^T \mathbf{MBv} \end{aligned} \quad (17)$$

Since $\mathbf{M}^T \mathbf{M} = \mathbf{F}^T \mathbf{C}^2 \geq 0$ and $\lambda_{\max}(\mathbf{A}_0) \leq 0$

$$\begin{aligned} \dot{V}(\mathbf{e}) &\leq \|\mathbf{S}\| \|\mathbf{Mf}\| + \mathbf{S}^T \mathbf{MBv} \\ &= \|\mathbf{S}\| \|\mathbf{Mf}\| - \left(\rho \|\mathbf{S}\| \|\mathbf{MB}\| + \eta \left(\frac{1}{2} \right)^\beta \|\mathbf{S}\|^{2\beta} \right) \end{aligned}$$

If $\rho \mathbf{MB} \geq \mathbf{Mf}$ and $\mathbf{S} \neq 0$

$$\dot{V}(\mathbf{e}) \leq -\eta \left(\frac{1}{2} \right)^\beta \|\mathbf{S}\|^{2\beta} < 0 \quad (18)$$

Therefore, the $\lim_{t \rightarrow \infty} \mathbf{e}(t) = 0$ [16, 17, 19, 29]. Since the model is an uncertain system, the new sliding mode observer for the system is robust.

Dividing (17) by (16) yields [29]

$$\frac{\dot{V}(\mathbf{e})}{2V(\mathbf{e})} \geq \frac{\mathbf{e}^T \mathbf{M}^T \mathbf{M} \mathbf{A}_0 \mathbf{e} - \eta((1/2)^\beta \|\mathbf{S}\|^{2\beta})}{\mathbf{e}^T \mathbf{M}^T \mathbf{M} \mathbf{e}} \quad (19)$$

Therefore

$$V(\mathbf{e}) \leq V(\mathbf{e}_0) e^{(h-\theta)t} \quad (20)$$

where h is $\lambda_{\max}(\mathbf{A}_0)$, θ is a positive number which is related to $\eta((1/2)^\beta \|\mathbf{S}\|^{2\beta})$. The converging rate is not $< e^{(h-\theta)}$.

3.3 Discrete observer design

3.2.1 Parameters design: The matrixes \mathbf{G} , \mathbf{M} and the coefficient ρ are the designed parameters of the new observer. If \mathbf{G} meets Assumption 1, and \mathbf{M} and ρ meet Assumption 2, the observer is robust.

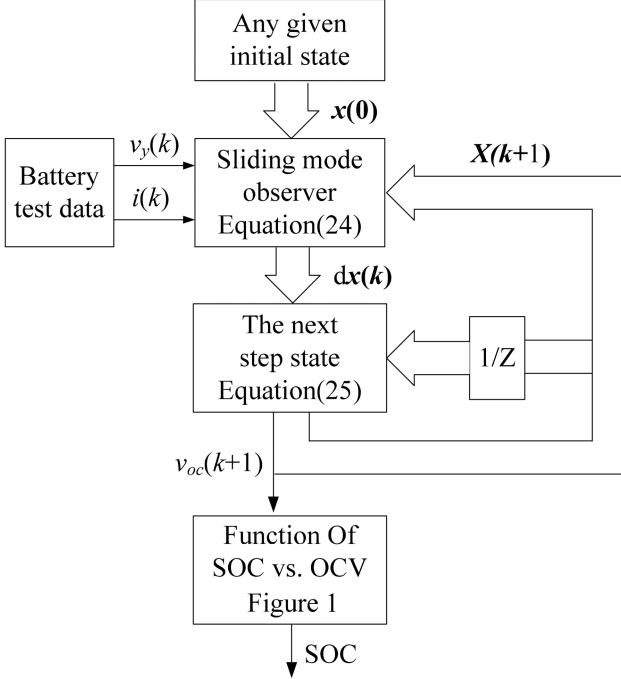


Fig. 3 Overall SOC estimation algorithm

(i) *The design of the matrix \mathbf{G} :* To the second-order model, the coefficient matrix $\mathbf{A} = \text{diag}(-(1/R_1C_1), -(1/R_2C_2), 0)$. \mathbf{G} is designed as 0, according to $\mathbf{A}_0 = \mathbf{A} - \mathbf{G}\mathbf{C}$, then $\mathbf{A}_0 = \mathbf{A}$, so Assumption 1 is met.

To the RC model, the coefficient matrix

$$\mathbf{A} = \begin{bmatrix} -\frac{1}{C_p(R_e + R_p)} & \frac{1}{C_p(R_e + R_p)} \\ \frac{1}{Q_n(R_e + R_p)} & -\frac{1}{Q_n(R_e + R_p)} \end{bmatrix}, \quad \text{and}$$

$$\mathbf{C} = \begin{bmatrix} R_e & R_p \\ R_e + R_p & R_e + R_p \end{bmatrix}.$$

\mathbf{G} is designed as $[(1/C_pR_p); -(1/Q_nR_p)]$, according to $\mathbf{A}_0 = \mathbf{A} - \mathbf{G}\mathbf{C}$, then

$$\mathbf{A}_0 = \begin{bmatrix} -\frac{1}{C_pR_p} & 0 \\ \frac{1}{Q_n} & 0 \end{bmatrix}$$

so Assumption 1 is met.

(ii) *The design of the matrixes \mathbf{M} , \mathbf{F} and the coefficient ρ :* \mathbf{M} and \mathbf{F} are the coefficient matrixes of the sliding mode surface (14), and they meet $\mathbf{M} = \mathbf{F}\mathbf{C}$. \mathbf{F} is designed as 1 in this paper. If the battery model is the second-order model, then $\mathbf{C} = [1 \ 1 \ 1]$ and $\mathbf{M} = [1 \ 1 \ 1]$. If the battery model is the RC model, then $\mathbf{C} = [(R_e/(R_e + R_p)) \ (R_p/(R_e + R_p))]$ and $\mathbf{M} = [(R_e/(R_e + R_p)) \ (R_p/(R_e + R_p))]$.

The coefficient matrixes \mathbf{B} and \mathbf{M} have been obtained. According to Assumption 2, ρ is determined by the uncertain function f . The states cannot be measured in the test, so the accurate f is unable to be obtained. For the sliding mode observer is robust, it is not necessary to know the accurate f , and we only need to know the range of it, which is the advantage of the observer. Through analysing the errors of the models, we first pre-estimate the range of f and pre-design ρ based on Assumption 2, then the pre-designed ρ is substituted in the observer, and we use the trying method to ensure the robustness of the observer.

Here, ρ contributes to the magnitude of the switch controller, and the increase of ρ usually enhances the robustness, but it also increases the chattering of the estimator. Considering the two factors, we pre-design $\rho = 10$ for the observer based on the two models, and the estimation results show the observer is robust.

In the two models or the other common battery models in this paper, \mathbf{M} is a row vector, and \mathbf{B} and f are column vectors, and according to Assumption 2, the calculation in the design of ρ is simple.

3.2.2 Discrete form of the new observer: We in this paper use the Taylor's series expansion for the discrete form of the observer [29]. The first-order Taylor's series expansion is

$$\hat{\mathbf{x}}(\mathbf{k} + 1) = \hat{\mathbf{x}}(\mathbf{k}) + \dot{\hat{\mathbf{x}}}(\mathbf{k}) \cdot \Delta t + o(\Delta t) \quad (21)$$

where $o(\Delta t)$ is a higher-order infinitesimal of the first-order derivative term, so it decreases with higher-order rate of the sampling period [30]. When the sampling period is short enough to neglect $o(\Delta t)$, the discrete form of the observer can be expressed as

$$\begin{cases} \mathbf{S}(\mathbf{k}) = \mathbf{M}(\hat{\mathbf{x}}(\mathbf{k}) - \mathbf{x}(\mathbf{k})) = \mathbf{F}(\hat{\mathbf{y}}(\mathbf{k}) - \mathbf{y}(\mathbf{k})) \\ \mathbf{v}(\mathbf{k}) = \begin{cases} -\frac{(\mathbf{S}(\mathbf{k})^T \mathbf{MB})^T}{\|\mathbf{S}(\mathbf{k})^T \mathbf{MB}\|^2} (\nabla_1(\mathbf{k}) + \nabla_2(\mathbf{k})) & \|\mathbf{S}(\mathbf{k})^T \mathbf{MB}\| \neq 0 \\ 0 & \|\mathbf{S}(\mathbf{k})^T \mathbf{MB}\| = 0 \end{cases} \\ d\hat{\mathbf{x}}(\mathbf{k}) = \mathbf{A}\hat{\mathbf{x}}(\mathbf{k}) + \mathbf{B}\mathbf{u}(\mathbf{k}) - \mathbf{G}(\mathbf{C}\hat{\mathbf{x}}(\mathbf{k}) - \mathbf{y}(\mathbf{k})) + \mathbf{B}\mathbf{v}(\mathbf{k}) \end{cases} \quad (22)$$

where $\nabla_1(\mathbf{k}) = \rho\mathbf{S}(\mathbf{k})\mathbf{MB}$ and $\nabla_2(\mathbf{k}) = \eta((1/2))^\beta\mathbf{S}(\mathbf{k})^{2\beta}$. Let $\eta = 1$ and $\beta = 0.95$ in this paper

$$\hat{\mathbf{x}}(\mathbf{k} + 1) = \hat{\mathbf{x}}(\mathbf{k}) + \dot{\hat{\mathbf{x}}}(\mathbf{k}) \cdot \Delta t \quad (23)$$

This discrete method will create the discrete error due to neglecting $o(\Delta t)$. In the state equations, let f' be the sum of the discrete error caused by $o(\Delta t)$ and all the other errors. If the discrete error is small enough to make f' meet Assumption 2, the sliding mode observer is still stable. The sampling period, in this paper, is 1 s, and the estimation results show that the discrete observer based on the two models is still robust. The whole SOC estimation algorithm is shown in Fig. 3.

4 Experiment

The test battery is a lithium-ion battery with 25 Ah nominal capacity. The test platform includes the Arbin BT2000 battery test system for the charge and discharge, the thermostat, the host computer and the corresponding monitoring software. The battery test system is controlled by the host computer. The host computer has the functions of setting battery operating conditions through compiling program in advance, and collecting and storing the measured data such as current and voltage. The thermostat is to maintain the environmental temperature around the battery. The battery was tested under the following two conditions with the test platform.

Condition 1: At room temperature, the battery, whose SOC = 100%, was tested under the simulation LA92 condition, until the terminal voltage reached the cut-off voltage of 3.0 V. Since the condition includes charge process and discharge process, the capacity of 1 Ah was discharged with C/3 current rate at beginning, lest the battery was overcharged. The test platform recorded the current and voltage in real-time with the sampling period of 1 s. The battery current and the terminal voltage under the simulation LA92 condition are shown in Figs. 4a and b.

Condition 2: At room temperature, the battery, whose SOC = 0, was charged with C/3 current rate, and when the terminal voltage reached 4.2 V, the charge mode converted to the constant voltage mode, during which the charge current gradually decreased. When the current rate reached C/30, the test was stopped, and now the

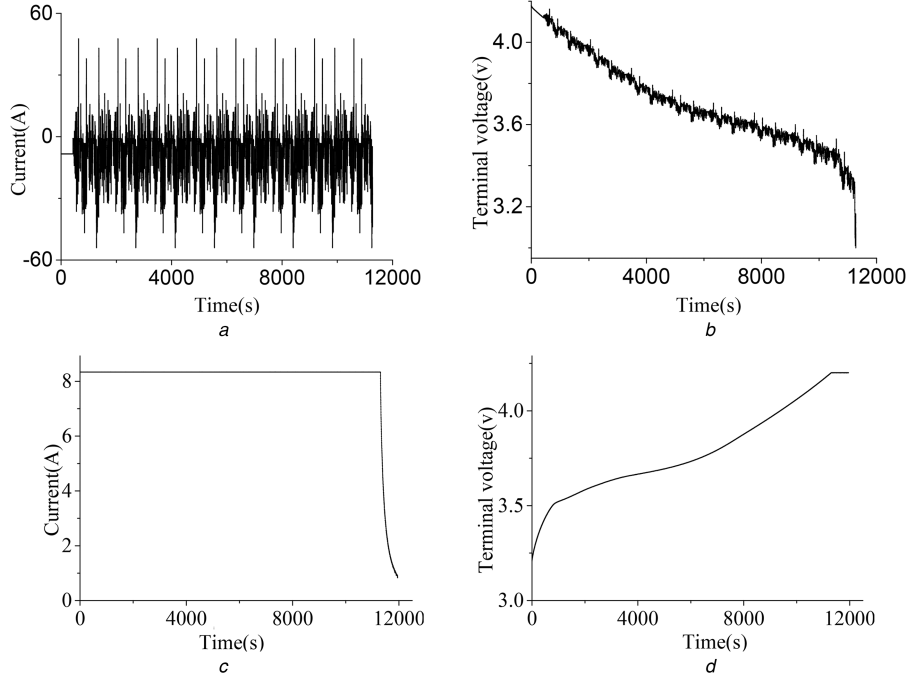


Fig. 4 Current and the terminal voltage under the two conditions

(a) Current under the simulation LA92, (b) Terminal voltage under the simulation LA92, (c) Charge current
(d) Terminal voltage under the charge

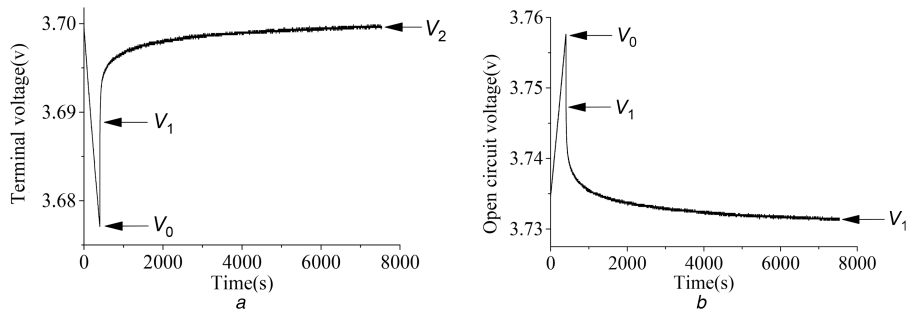


Fig. 5 Terminal voltage after the current pulses

(a) After the discharge pulse, (b) After the charge pulse

Table 1 Parameters of the second-order model

Parameters	R_i , mΩ	R_1 , mΩ	C_1 , F	R_2 , mΩ	C_2 , F
values	1.24	1.31	4.6×10^{-4}	0.15	2.4×10^{-4}

SOC was defined as 100%. The charge current and the terminal voltage are shown in Figs. 4c and d.

4.1 Model parameters identification

The parameters of the battery models can be extracted by the current pulses. When the SOC is 53.7%, the battery terminal voltage after the discharge pulse is shown in Fig. 5a, and when the SOC is 56.3%, the battery terminal voltage after the charge pulse is shown in Fig. 5b.

As shown in Fig. 5a, in the second-order circuit model, the ohmic resistance $R_i = ((V_1 - V_0)/\nabla i)$, and the time constants of the two RC parallel branches are $\tau_1 = R_1 C_1$ and $\tau_2 = R_2 C_2$. After the discharge pulse, the battery terminal voltage is

$$V_t = V_1 + iR_1(1 - e^{-(t/\tau_1)}) + iR_2(1 - e^{-(t/\tau_2)}) \quad (24)$$

According to the measured data for 10 s after the pulse discharge, and using the least-square method, we obtained that $R_1 = 1.24 \text{ m}\Omega$, $R_2 = 1.24 \text{ m}\Omega$, $\tau_1 = 60.6 \text{ s}$ and $\tau_2 = 3.6 \text{ s}$. According to $C_1 = \tau_1/R_1$

and $C_2 = \tau_2/R_2$, C_1 and C_2 can be obtained. The identification results of the model parameters are shown in Table 1.

In the RC circuit model, if the internal resistance is R^* , then $R^* = R_i + ((1/R_e) + (1/R_p))^{-1}$. We usually let $R_e = 3R_i$ [26]. Through analysing the model and the discharge pulse curve in Fig. 5a, we obtained $R^* = ((V_1 - V_0)/\nabla i)$, and $(R_e/(R_e + R_p))R_e = ((V_2 - V_1)/\nabla i)$, so the resistances in the RC circuit model are

$$\begin{cases} R_i + \left(\frac{1}{R_e} + \frac{1}{R_p}\right)^{-1} = 1.24 \\ \frac{R_e}{R_e + R_p}R_e = 1.46 \\ R_e = 3R_i \end{cases} \quad (25)$$

If the time constant is τ , the battery terminal voltage after pulse discharge can be expressed as

$$V_t = V_1 + (V_2 - V_1)(1 - e^{-(t/\tau)}) \quad (26)$$

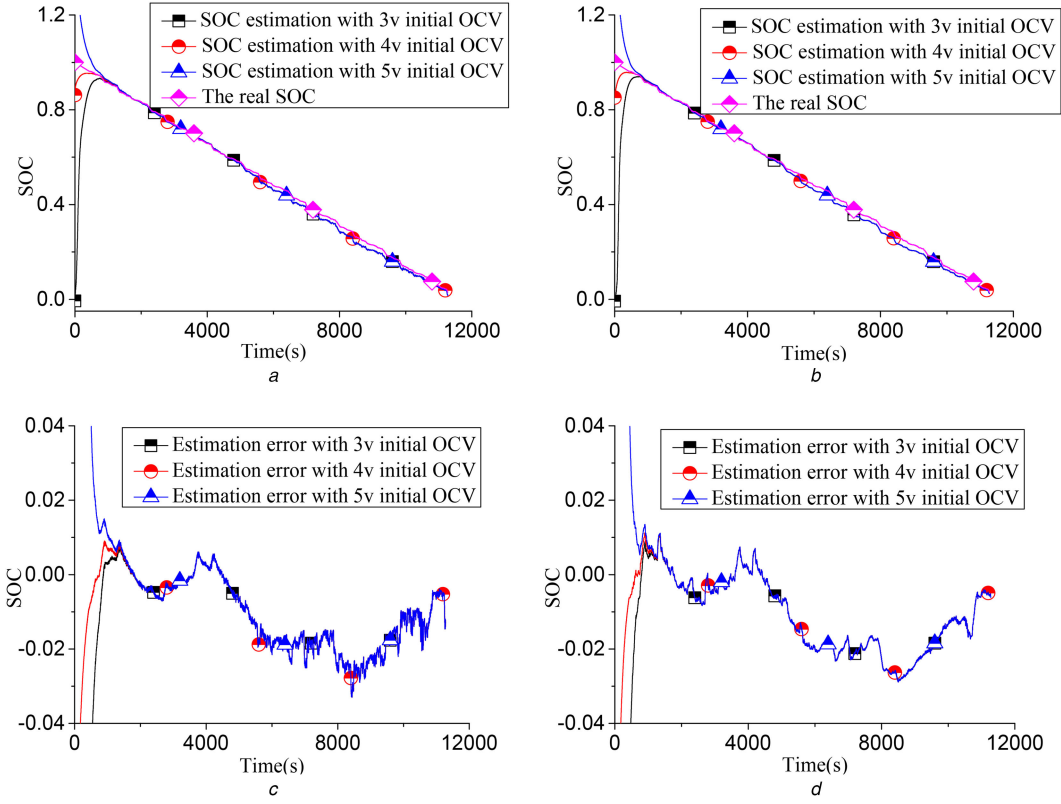


Fig. 6 SOC estimation and estimation errors by the new observer

(a) On the basis of the second-order circuit model, (b) On the basis of the RC circuit model, (c) On the basis of the second-order circuit model, (d) On the basis of the RC circuit model

According to the measured data for 10 s after the pulse discharge, and using the least-square method, we obtained $\tau = 34.2$ s. The capacitance C_p can be obtained through the following equation:

$$C_p = \frac{\tau}{R_e + R_p} \quad (27)$$

The identification results of the model parameters are shown in Table 2.

4.2 SOC estimation of the simulation LA92 condition

When using the new observer to estimate the SOC under the simulation LA92 condition, the initial state, within the stable range of the observer, can be set as an arbitrary value. If the model is the second-order circuit model, the initial state vector is set as $x_0 = [0; 0; 5]$, $[0; 0; 4]$ and $[0; 0; 5]$, and if the model is the RC circuit model, the initial state vector is set as $x_0 = [3; 3]$, $[4; 4]$ and $[5; 5]$.

After the simulation LA92 condition test, we obtained that the residual capacity was 0.78 Ah with the OCV method. According to (1), the true SOC can be obtained through current integration in real-time. When choosing $\eta = 1$, the sum of the calculated discharge capacity with current integration and the residual capacity was almost equal to Q_n , so η was set as 1. The SOC estimation can be obtained through the new observer and the OCV curve fitted with the OCV data during the discharge process in Fig. 1. The SOC estimation results are shown in Figs. 6a and b and the estimation errors are shown in Figs. 6c and d.

Fig. 6 indicates that though the initial values of the state vector are different, the SOC estimation results based on the same model have almost the same convergence value. For the battery models

are the uncertain systems, so the new observer is robust. The SOC estimation errors in Figs. 6c and d are no more than 3.30 and 2.89%, respectively, when the initial state vector is set as the above values. When the initial state vector is set as the other values, approximately equal convergence results to those in this paper can be obtained.

The disadvantage of the sliding mode observer is that the discontinuous change of the switch controller causes the fast oscillations. The fast oscillations can arouse the unmodelled dynamics, which will enlarge the estimation error. Increasing the switch amplitude enhances the robustness, but it enlarges the oscillations. The Kalman filter does not cause the oscillations, and it can eliminate the effect of the model noise on the estimation result. The estimation errors by the Kalman filter are shown in Fig. 7.

Figs. 7a and b are the estimation errors based on the second-order model and the RC model, and they are no more than 2.80 and 2.52%, respectively. From Figs. 6c and 7a, it is obvious that the sliding mode observer causes the fast oscillations in the presence of unmodelled dynamics.

However, the Kalman filter is not robust, and the model has great impact on the estimation result. For example, the covariance of the model noise must be known when using the Kalman filter, but it is difficult to get the covariance. By comparison with the Kalman filter, the new observer is robust and only needs to know the ranges of the model errors.

On the basis of the other common circuit models in this paper, the new sliding mode observer also can be used for battery SOC estimation, and the design method is same as the above method.

4.3 SOC estimation of the charge process

The OCV in the charge process is shown in Fig. 1. According to Fig. 5b, we can obtain the parameters of the two circuit models during the charge process with the identification method in Section 4.1. The identification results of the parameters are shown in Tables 3 and 4. From Fig. 1 and Tables 1–4, it can be seen that the charge parameters are different to the discharge parameters.

Table 2 Parameters of the RC circuit model

Parameters	C_p , F	R_i , mΩ	R_e , mΩ	R_p , mΩ
values	1.2×10^4	0.68	2.03	0.78

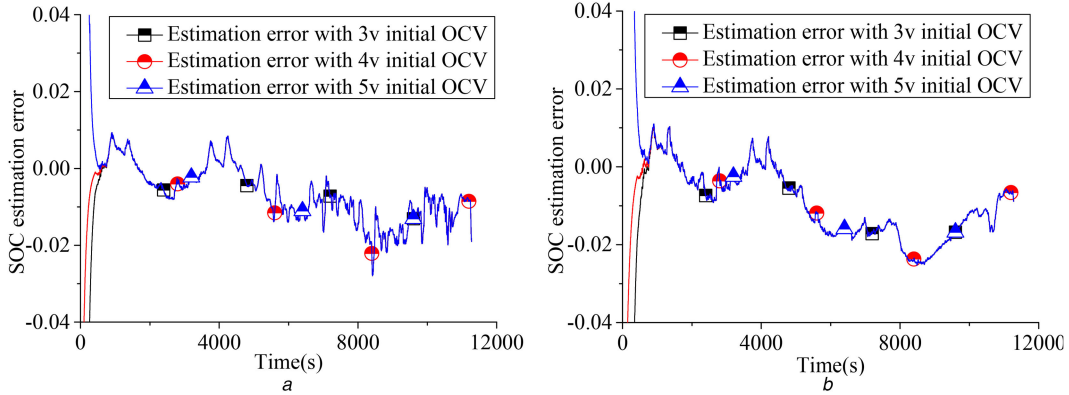


Fig. 7 Estimation errors by the Kalman filter

(a) On the basis of the second-order circuit model, (b) On the basis of the RC circuit model

Table 3 Parameters of the second-order circuit model

Parameters	R_p , mΩ	R_i , mΩ	C_1 , F	R_2 , mΩ	C_2 , F
values	1.24	1.77	3.5×10^4	0.15	3.4×10^4

Table 4 Parameters of the RC circuit model

Parameters	C_p , F	R_i , mΩ	R_e , mΩ	R_p , mΩ
values	1.4×10^4	0.79	2.37	0.56

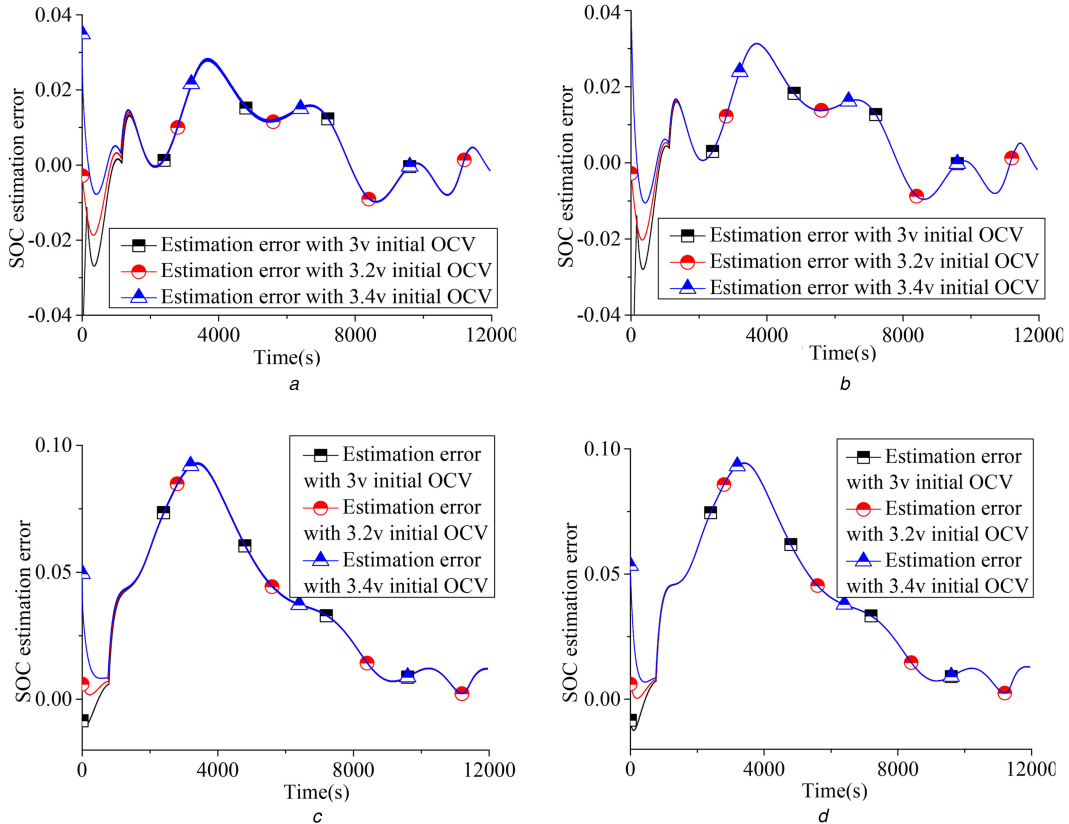


Fig. 8 SOC estimation errors in the charge process

(a) Second-order circuit model of charge parameters, (b) RC circuit model of charge parameters, (c) Second-order circuit model of discharge parameters, (d) RC circuit model of discharge parameters

The SOC estimation errors of the charge test by the new observer are shown in Fig. 8. Figs. 8a and b show the estimation errors with the charge parameters, where (a) is based on the second-order circuit model and (b) is based on the RC circuit model, and they are no more than 2.84 and 3.14%, respectively. Figs. 8c and d show the estimation errors with the discharge parameters, where (c) is based on the second-order model and (d)

is based on the RC model, and they are no more than 9.32 and 9.44%, respectively.

The charge test indicates that the observer with the charge parameters can accurately estimate the SOC and that the observer obviously increases the estimation errors with the discharge parameters. Therefore, the SOC estimation during the charge process requires another measurement of the OCV and identification of the model parameters.

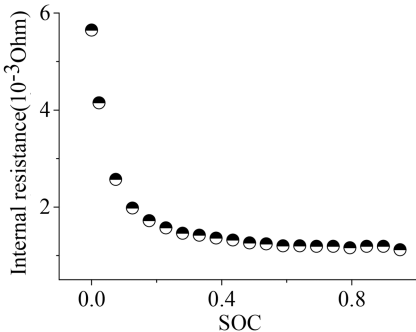


Fig. 9 Internal resistance versus SOC

4.4 SOC estimation with an adaptive new sliding mode observer

SOC estimation is affected by the accuracy of battery model, and the model parameters change with SOC, temperature and current rate. Experimental analysis shows that, among the model parameters, the internal resistance has mainly influence on the SOC estimation in the test. The functional relationship between the internal resistance R^* and the SOC, the temperature and the current is $R^* = R^*(S_{oc}, T, i)$.

The test was operated in the thermostat, so the influence of temperature is neglected. The test battery is power-type battery, and it was proved through tests that the current has little effect on the battery internal resistance. From the above analysis, the function $R^* = R^*(S_{oc}, T, i)$ in the test can be simplified as $R^* = R^*(S_{oc})$. The change of the internal resistance with the SOC, drawn by measuring, is shown in Fig. 9.

The algorithm of loop iteration used in SOC estimation is an adaptive algorithm. During the calculation, the model parameters are identified with the estimated SOC, and the identified parameters are used for SOC estimation [18, 24]. Since the model parameters are updated in real-time in the estimation process, the model accuracy is improved. The proving process in Section 3.2 shows that the new sliding mode observer can be used for the state

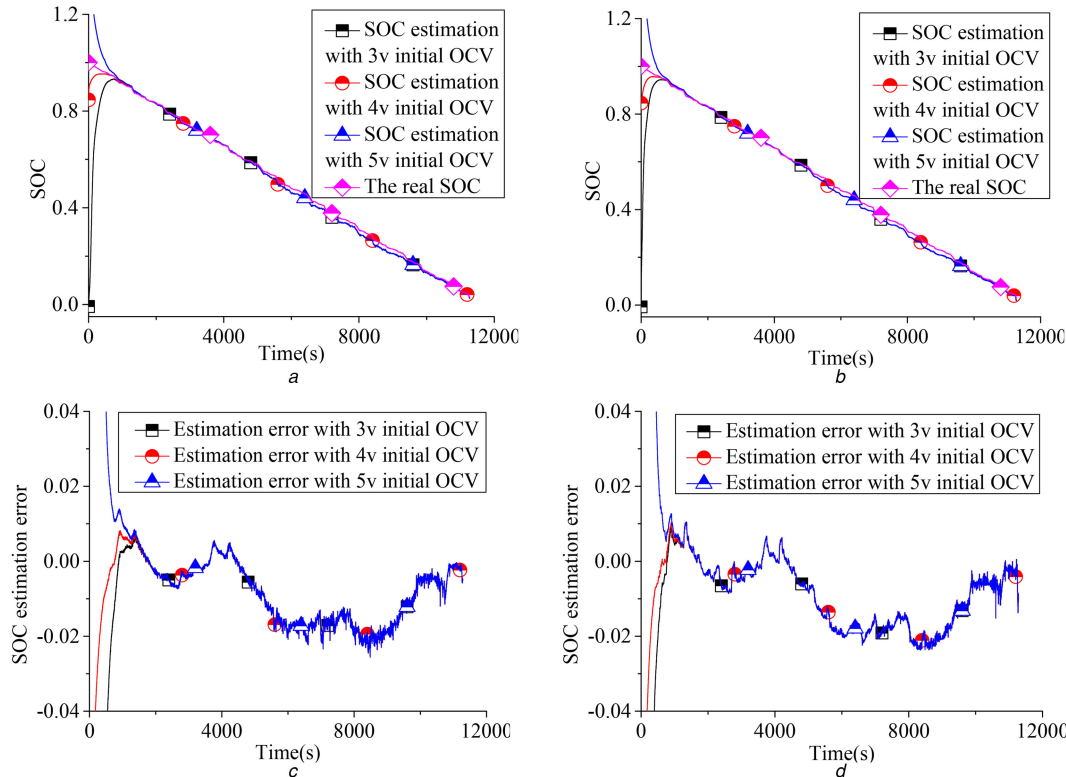


Fig. 10 SOC estimation and the estimation errors with the adaptive new observer

(a) On the basis of the second-order circuit model, (b) On the basis of the RC circuit model, (c) On the basis of the second-order circuit model, (d) On the basis of the RC circuit model

estimation of time-varying battery system. In this paper, the battery state equation time-varying coefficient is $R^*(S_{oc})$, and the design of the observer based on time variable parameter model is similar to that based on time-invariant parameter model. Using the same design method with Section 3.3, the designed coefficients of the adaptive observer can be designed as the same values with those of the above observer, and the adaptive observer is robust.

When the initial values are the above values, the SOC estimation and estimation errors with the adaptive new observer under the simulation LA92 condition are shown in Fig. 10. Fig. 10 indicates that the adaptive new sliding observer is robust, and the estimation errors, as shown in Figs. 10c and d, are no more than 2.56 and 2.37%, respectively. When the initial values are the other values, the approximately equal estimation results to those in this paper can be obtained. By comparing Figs. 10c and d with Figs. 7c and d, it can be concluded that the adaptive observer improves the accuracy of estimation.

Owing to the influence of measurement accuracy, the non-linear characteristic of batteries and the parameters identification errors, it is not sure that the estimation of which case of the observer based on the two models is more accurate, but it is demonstrated that the adaptive approach improves the accuracy of the battery model and the SOC estimation through the test.

5 Conclusions

- i. A new sliding mode observer is designed for SOC estimation and its robustness is proved by Lyapunov's stability and the simulation LA92 condition test. The design processes show that the design of the new observer is simple and the observer exhibits good generality.
- ii. The new sliding mode observer can be used for the SOC estimation of both time-varying system and time-invariant system, and the adaptive method applied for the SOC estimation of time-varying system can update model parameters in real-time, which improves the accuracy of the battery model and the SOC estimation.
- iii. When considering the change of the other model parameters, the design method is same with the method in this paper.

- iv. The battery model is very important to SOC estimation, and the model parameters are changing with the temperature and state of health (SOH). The SOC estimation under the conditions of different temperature and SOH needs to know the variation rule of the parameters with the temperature and SOH, so it is necessary to further study the features of batteries affected by temperature and ageing in the future.

6 Acknowledgment

The work was supported by the National Natural Science Foundation of China (no. 51477009).

7 References

- [1] Ng, K.S., Moo, C.-S., Chen, Y.-P., *et al.*: ‘Enhanced coulomb counting method for estimating state-of-charge and state-of-health of lithium-ion batteries’, *Appl. Energy*, 2009, **86**, pp. 1506–1511
- [2] Piller, S., Perrin, M., Jossen, A.: ‘Methods for state-of-charge determination and their applications’, *J. Power Sources*, 2001, **96**, pp. 113–120
- [3] Gholizade-Narm, H., Charkhgard, M.: ‘Lithium-ion battery state of charge estimation based on square-root unscented Kalman filter’, *IET Power Electron.*, 2013, **6**, (9), pp. 1833–1841
- [4] Plett, G.L.: ‘Extended Kalman filtering for battery management systems of LiPB-based HEV battery packs part 3 state and parameter estimation’, *J. Power Sources*, 2004, **134**, pp. 277–292
- [5] Plett, G.L.: ‘Sigma-point Kalman filtering for battery management systems of LiPB-based HEV battery packs part 1: introduction and state estimation’, *J. Power Sources*, 2006, **161**, pp. 1356–1368
- [6] Plett, G.L.: ‘Sigma-point Kalman filtering for battery management systems of LiPB-based HEV battery packs part 2: simultaneous state and parameter estimation’, *J. Power Sources*, 2006, **161**, pp. 1369–1384
- [7] Aylor, J., Thieme, A., Johnson, B.: ‘A battery state of charge indicator for electric wheelchairs’, *IEEE Trans. Ind. Electron.*, 1992, **39**, pp. 398–409
- [8] Cheng, B., Bai, Z., Cao, B.: ‘State of charge estimation based on evolutionary neural network’, *Energy Convers. Manage.*, 2008, **49**, pp. 2788–2794
- [9] Kang, L., Zhao, X., Ma, J.: ‘A new neural network model for the state-of-charge estimation in the battery degradation process’, *Appl. Energy*, 2014, **121**, pp. 20–27
- [10] Charkhgard, M., Farrokhi, M.: ‘State-of-charge estimation for lithium-ion batteries using neural networks and EKF’, *IEEE Trans. Ind. Electron.*, 2010, **57**, pp. 4178–4187
- [11] Shi, Q.-S., Zhang, C.-H., Cui, N.-X.: ‘Estimation of battery state-of-charge using v-support vector regression algorithm’, *Int. J. Autom. Technol.*, 2008, **9**, pp. 759–764
- [12] Jang, J.H., Yoo, J.Y.: ‘Impedance-based and circuit-parameter-based battery models for HEV power systems’, *Int. J. Autom. Technol.*, 2008, **9**, pp. 615–623
- [13] Charkhgard, M., Zarif, M.H.: ‘Design of adaptive H_∞ filter for implementing on state-of-charge estimation based on battery state-of-charge-varying modelling’, *IET Power Electron.*, 2015, **8**, pp. 1825–1833
- [14] Unterrieder, C., Zhang, C., Lunglmayr, M., *et al.*: ‘Battery state-of-charge estimation using approximate least squares’, *J. Power Sources*, 2015, **278**, pp. 274–286
- [15] Waag, W., Sauer, D.U.: ‘Adaptive estimation of the electromotive force of the lithium-ion battery after current interruption for an accurate state-of-charge and capacity determination’, *Appl. Energy*, 2013, **111**, pp. 416–427
- [16] Kim, I.: ‘The novel state of charge estimation method for lithium battery using sliding mode observer’, *J. Power Sources*, 2006, **163**, pp. 584–690
- [17] Gholizadeh, M., Salmasi, F.R.: ‘Estimation of state of charge, unknown nonlinearities, and state of health of a lithium-ion battery based on a comprehensive unobservable model’, *IEEE Trans. Ind. Electron.*, 2014, **61**, pp. 1335–1344
- [18] Unterrieder, C., Priewasser, R., Marsili, S., *et al.*: ‘Battery state estimation using mixed Kalman/ H_∞ , adaptive Luenberger and sliding mode observer’. Vehicle Power and Propulsion Conf., 2013, pp. 71–76
- [19] Chen, X., Shen, W., Cao, Z., *et al.*: ‘A novel approach for state of charge estimation based on adaptive switching gain sliding mode observer in electric vehicles’, *J. Power Sources*, 2014, **246**, pp. 667–678
- [20] Kim, I.: ‘A technique for estimating the state of health of lithium batteries through a dual-sliding-mode observer’, *IEEE Trans. Power Electron.*, 2010, **25**, pp. 1013–1022
- [21] Kim, I.: ‘Nonlinear state of charge estimator for hybrid electric vehicle battery’, *IEEE Trans. Power Electron.*, 2008, **23**, pp. 2027–2034
- [22] Gould, C.R., Bingham, C.M., Stone, D.A., *et al.*: ‘New battery model and state-of-health determination through subspace parameter estimation and state-observer techniques’, *IEEE Trans. Veh. Technol.*, 2009, **58**, pp. 3905–3916
- [23] Chen, X., Shen, W., Cao, Z., Kapoor, A.: ‘Adaptive gain sliding mode observer for state of charge estimation based on combined battery equivalent circuit model’, *Comput. Chem. Eng.*, 2014, **64**, pp. 114–123
- [24] Kim, D., Koo, K., Jeong, J.J., Goh, T., Kim, S.W.: ‘Second-order discrete-time sliding mode observer for state of charge determination based on a dynamic resistance li-ion battery model’, *Energies*, 2013, **6**, pp. 5538–5551
- [25] Kuhn, E., Forgez, C., Lagonotte, P., Friedrich, G.: ‘Modeling Ni-MH battery using Cauer and Foster structures’, *J. Power Sources*, 2006, **158**, pp. 1490–1497
- [26] Bhangu, B.S., Bentley, P., Bingham, C.M.: ‘Nonlinear observers for predicting state-of-charge and state-of-health of lead-acid batteries for hybrid-electric vehicle’, *IEEE Trans. Veh. Technol.*, 2005, **54**, pp. 783–794
- [27] Bao, S., Feng, Y., Sun, L.: ‘Robust sliding mode observer design of nonlinear uncertain systems’, *J. Harbin Inst. Technol.*, 2004, **36**, pp. 613–616
- [28] Zhang, N., Feng, Y., Qiu, D.: ‘Robust sliding mode observer design of nonlinear uncertain systems’, *Control Theory Appl.*, 2007, **24**, pp. 715–718
- [29] Walcott, B.L., Zak, S.H.: ‘State observation of nonlinear uncertain dynamical systems’, *IEEE Trans. Autom. Control*, 1987, **AC-32**, (2), pp. 166–170
- [30] Veluvolu, K.C., Soh, Y.C., Cao, W.: ‘Robust discrete-time nonlinear sliding mode state estimation of uncertain nonlinear systems’, *Int. J. Robust Nonlinear Control*, 2007, **17**, pp. 803–828